Electron spin transport in quantum dots and point contacts

Koop, Erik Johan

Chapter 5

Confinement-enhanced spin relaxation for electron ensembles in large quantum dots

We present a numerical study of spin relaxation in a semiclassical electron ensemble in a large ballistic quantum dot. The dot is defined in a GaAs/AlGaAs heterojunction system with a two-dimensional electron gas, and relaxation occurs due to Dresselhaus and Rashba spin orbit interaction. We find that confinement in a micronscale dot can result in strongly enhanced relaxation with respect to a free two-dimensional electron ensemble, contrary to the established result that strong confinement or frequent momentum scattering reduces relaxation. This effect occurs when the size of the system is on the order of the spin precession length, but smaller than the mean free path.

This chapter is based on Ref. 4 on p. 131.

5.1 Introduction

Due to spin-orbit interaction (SOI), the state of electron spins is influenced by electron transport in electronic devices. This has been recognized as a source for dephasing and relaxation for spins [1, 2], as well as a means for controlled spin manipulation [3] in research that aims at developing spintronic devices [2, 4, 5]. In this article we present a numerical study of spin relaxation in an electron ensemble that is scattering inside a micronscale device structure. We are interested in the case where devices are made of clean semiconductor heterostructures and studied at low temperatures. For our studies we assume realistic material parameters for a system with a two-dimensional electron gas (2DEG) at a GaAs/AlGaAs heterojunction. For a free 2DEG in these materials, a well established result is that the average spin orientation of an ensemble decays due to precession in spin-orbit fields. For moderate electron mobilities, this so-called D'yakonov-Perel' (DP) mechanism for spin relaxation [6, 7] has the property that the spin relaxation time T_1 increases when the mobility (and thereby the time scale τ_s for elastic momentum scattering) decreases, as $T_1 \propto \tau_s^{-1}$.

A similar trend is observed when the degree of electron confinement in a device structure is increased. Stronger confinement gives more frequent scattering on the boundaries of the system, and hence reduces the relaxation. This has been recognized in the increase of T_1 on the transition from 2D to 1D systems [8]. In the limit quantum confinement in extremely small devices (much smaller systems than we consider for the present study), relaxation and dephasing due to SOI is then strongly reduced, and other relaxation mechanisms can become dominant. This applies for example to spin dephasing in few-electron quantum dots, which can be mainly due to interaction with nuclear spins [10, 11, 9]. Although more frequent scattering due to stronger confinement thus seems similar to reducing the mobility in bulk materials, the results that we present here show that frequent scattering due to confinement can also result in the opposite, namely confinement-enhanced relaxation.

The key result of the present study is well presented by the traces for spin relaxation time T_1 as a function of the size L of a square quantum dot in Fig. 5.1a. The trace for the case that an external magnetic field $B_{ext} = 0$ T and 2DEG mobility $\mu = 100$ m^2/Vs, shows that T_1 is constant for $L > 10$ μm. Here L is so large that the electron ensemble behaves as in a free 2DEG. When decreasing L below 10 μm, T_1 increases because spin relaxation in suppressed by more frequent scattering on the edge of the system. The trace for $B_{ext} = 10$ T and

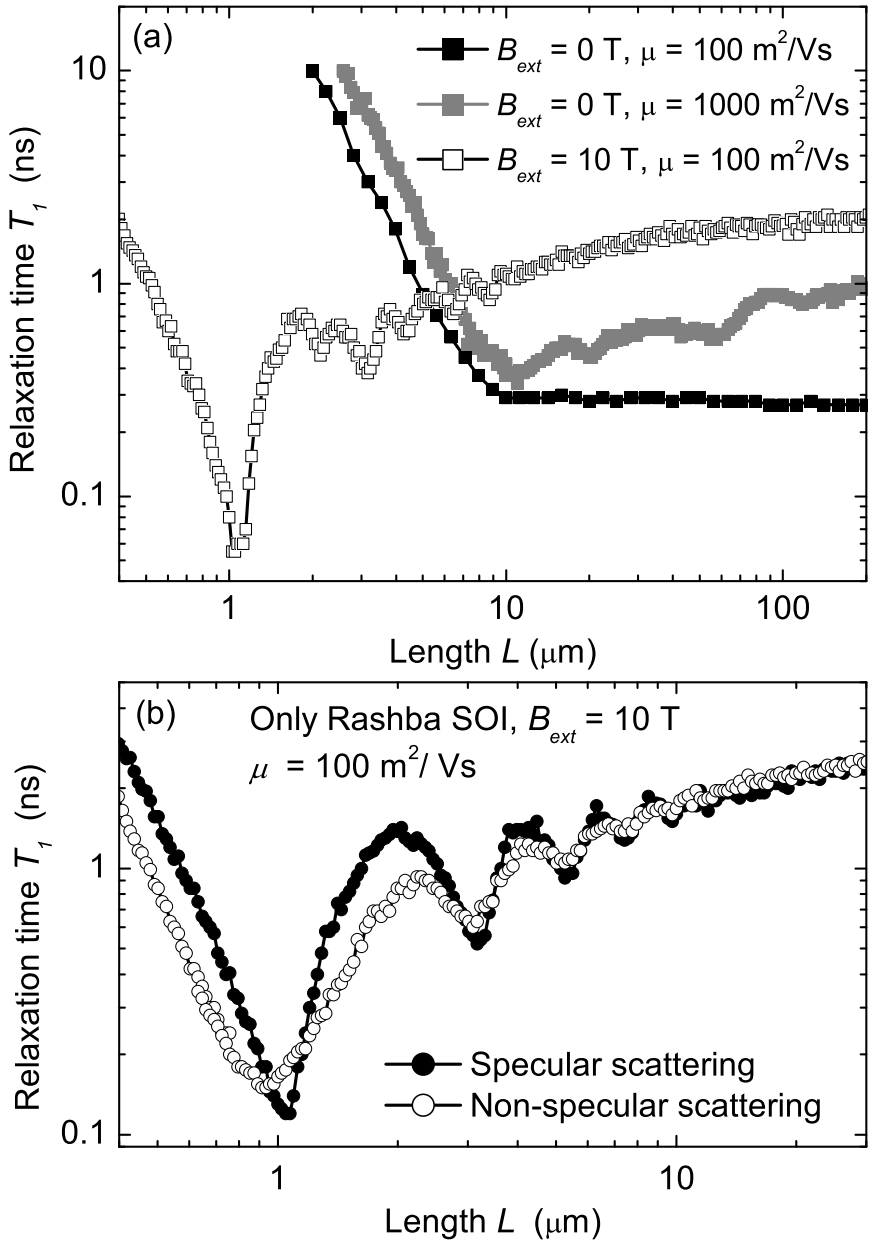

Figure 5.1: **(a)** Spin ensemble relaxation in a quantum dot system of size L. The relaxation time T_1 is calculated as a function the size L for a square system. For mobility $\mu = 100$ m^2/Vs we plot T_1 for zero external magnetic field (filled black symbols) and for $B_{ext} = 10$ T (open symbols). The gray symbols show T_1 for zero external magnetic field and $\mu = 1000$ m^2/Vs. **(b)** Relaxation time as a function of L for a system with only Rashba SOI. Calculations for specular and non-specular reflections give qualitatively the same results, but the magnitude of the resonant structure in the traces of T_1 as a function of L is larger in the case of specular reflections.

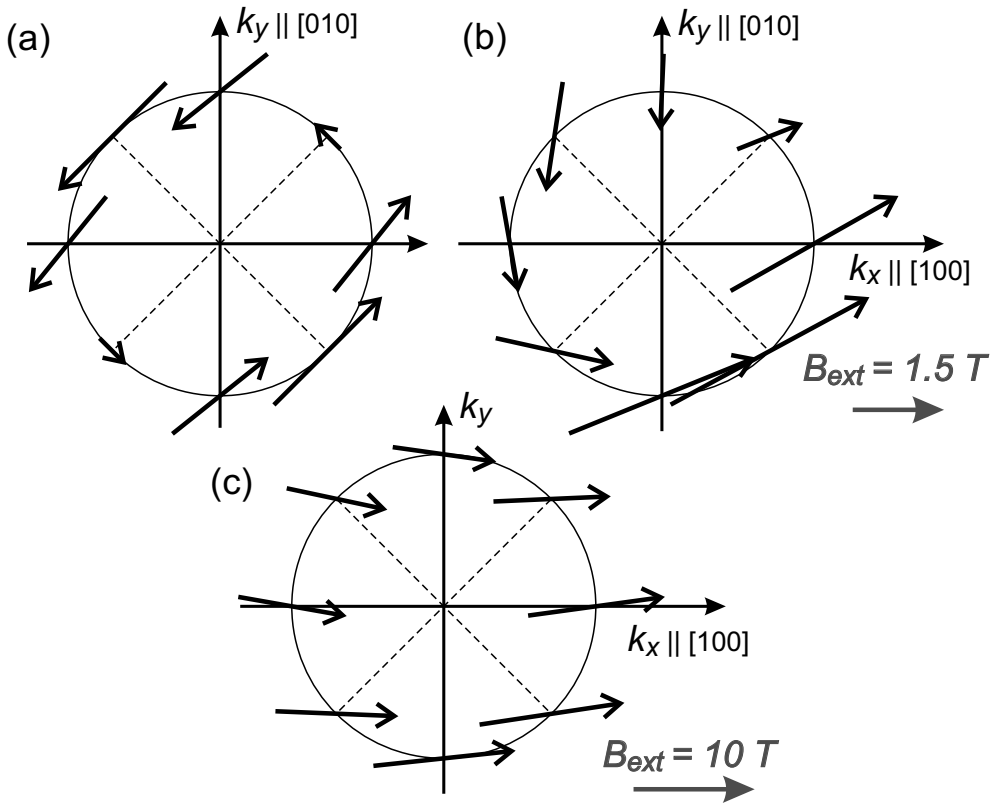

Figure 5.2: **(a)** Schematic representation of the direction and magnitude of the SOI fields. Since we assume all electrons move with the same magnitude for k-vector k_F, we can represent the motion of electrons in all directions as a circle in the (k_x,k_y)-plane. The arrows that are sketched at certain points on this Fermi circle, represent the strength and direction of the SO field $\mathbf{B}_{SO}$ for that k-vector. **(b)** Magnitude and direction of the total effective magnetic field when an external field $B_{ext} = 1.5$ T is applied along the [100]-direction. **(c)** Idem for an external field $B_{ext} = 10$ T. In this plot the length of all arrows has been scaled down by a factor 5 as compared to **(a)** and **(b)**.

2DEG mobility $\mu = 100$ m^2/Vs (typical parameters for research on spin effects in micronscale quantum dots [13] and wires [14]), however, shows radically different behavior. Now T_1 first slowly decreases when decreasing L from the 2D regime (very large L), and shows a pronounced dip for $L \approx 1$ μm. Confinement now strongly enhances relaxation, instead of the more familiar result that confinement reduces relaxation. Moreover, in the range with 1 μm $< L <$ 10 μm, T_1 has a highly structured dependence on L. Only when decreasing L below $L \approx 1$ μm, T_1 shows again a strong and monotonic increase as for the confinement-suppressed

relaxation in $B_{ext} = 0$ T.

We obtain these results with a numerical Monte Carlo approach. This has the advantage that we can study precessional relaxation for realistic conditions, where the total magnetic field is the sum of several spin-orbit contributions and an external field. In reality, samples typically have both Rashba and Dresselhaus SOI that are comparable in magnitude [15], and in experiments one often needs to apply strong external magnetic fields for realizing spin transport in non-magnetic semiconductors [16, 13, 14]. The combination of spin-orbit contributions and external magnetic fields may strongly influence the relaxation behavior in these type of devices [17, 18]. Earlier studies of these relaxation phenomena were often restricted to more tractable cases, as for example with only Rashba SOI [19] (no Dresselhaus SOI), and no external fields. Below, we will summarize our numerical method, and then focus on studying the dependence of T_1 on the degree of confinement in micronscale quantum dots. We will also show that in regimes and for parameters that were studied before, our simulations give the conventional results.

5.2 Spin-orbit coupling

We use a description where spin-orbit (SO) coupling acts as a k-vector dependent effective magnetic field on the electron spins. In a 2DEG it is dominated by two sources [15]. The first arises due to the inversion asymmetry in the potential profile of the heterostructure and results in an effective Rashba magnetic field $\mathbf{B}_R$ [20]. The second effect arises due to the lack of inversion symmetry in the GaAs crystal lattice, which is of the zinc-blende type, and yields for a 2DEG the linear and cubic Dresselhaus fields $\mathbf{B}_{D1}$ and $\mathbf{B}_{D3}$ [21, 1]. The effective SO field $\mathbf{B}_{SO}$ in a 2DEG can thus be described as the vector sum of these three components, given by [15, 1]

$$\mathbf{B}_R = C_R(\hat{\mathbf{x}}k_y - \hat{\mathbf{y}}k_x), \tag{5.1}$$

$$\mathbf{B}_{D1} = C_{D1}(-\hat{\mathbf{x}}k_x + \hat{\mathbf{y}}k_y), \tag{5.2}$$

$$\mathbf{B}_{D3} = C_{D3}(\hat{\mathbf{x}}k_x k_y^2 - \hat{\mathbf{y}}k_y k_x^2), \tag{5.3}$$

where C_R, C_{D1} and C_{D3} are the coupling parameters, $\hat{\mathbf{x}}$ is the unit vector in the [100]-direction, and $\hat{\mathbf{y}}$ in the [010]-direction. Our results are calculated using the SO parameters that were reported by Miller *et al.* [15], $C_R = -1.96 \cdot 10^{-8}$ Tm, $C_{D1} = -1.57 \cdot 10^{-8}$ Tm, and $C_{D3} = -1.18 \cdot 10^{-24}$ Tm^3.

The total SO field is then anisotropic in momentum space as is shown in Fig. 5.2a. Each time an electron scatters and its direction of motion changes it will precess around a different axis set by $\mathbf{B}_{SO}$. For our set of SO parameters these fields $\mathbf{B}_{SO}$ lie more or less parallel to the [110]-direction for almost all k-directions. Figures 5.2b,c show the effect of adding an external magnetic field $\mathbf{B}_{ext}$, which is independent of momentum direction. We consider here the situation that $\mathbf{B}_{ext} \parallel \hat{\mathbf{x}}$. The total effective magnetic field $\mathbf{B}_{tot}$ is then the vector sum of the SO fields and the external magnetic field. When the magnitude B_{ext} of $\mathbf{B}_{ext}$ is comparable to that of the SO fields, as shown in Fig. 5.2b for $B_{ext} = 1.5$ T, the total effective magnetic fields are no longer mainly parallel to the [110]-direction and there is larger spread in the directions of the precession axes $\mathbf{B}_{tot}$. Figure 5.2c shows that for very large external magnetic fields, shown here for $B_{ext} = 10$ T, the total effective magnetic fields $\mathbf{B}_{tot}$ align with $\mathbf{B}_{ext}$ along the [100]-direction. This again reduces the spread in the direction of the precession axes $\mathbf{B}_{tot}$.

5.3 Method

In our numerical approach we use a classical description of the electron motion, and a quantum mechanical description of the dynamics of the electron spin. We thus assume that electrons have at all times a well-defined k-vector, and electrons move along classical trajectories with specular scattering on the boundaries of the system, and scattering in a random direction on static potential fluctuations due to impurities. Electrons never escape from the system. Although in micronscale quantum dots the motion of electrons is confined, the mean level spacing is much smaller than temperature, $\Delta_m \ll k_B T$, and this allows for this semiclassical description. Further, we consider the case that all the electrons that carry the spin orientation are near the Fermi level. Thus, we assume that all electron always move with the Fermi velocity (k-vectors with magnitude k_F), independent of the momentum direction. This is a valid approximation for $k_B T, \Delta E_{Z,SO} \ll E_F$ (with respect to the bottom of the conduction band), where $\Delta E_{Z,SO}$ is the Zeeman splitting due to the SO field alone. Obviously, the validity of our approach breaks down in the limit of very small dots, where electrons are highly localized due to quantum confinement. In practice, this occurs for quantum dots with size L below ~ 400 nm, but our results for this regime always show a very strong suppression of precessional relaxation, which is the semiclassical equivalent for suppressed relaxation for quantum confined electrons [10, 11].

Our simulation then works as follows. It starts at $t = 0$ with each electron

at a random position in a square shaped dot of size L, and with a k-vector in a random direction. We always consider the case that at $t = 0$ the spin state is prepared in the positive $\hat{\mathbf{x}}$-direction. For each electron, we follow its state in time, and its momentum direction will change at each scattering event. During each ballistic trajectory between scatter events, the electron has a well-defined k-vector, and we calculate the effective spin-orbit field during this trajectory with Eqs. 5.1-5.3. The precession angle α_i during a single trajectory is then given by

$$\alpha_i = \frac{g\mu_B \mathbf{B}_{tot}}{\hbar} \cdot t_i, \tag{5.4}$$

where t_i is the traveling time $t_i = l_i/|v|$. The rotation operator working on the initial spin state to determine the new spin state is a function of α_i and of the unit vector $\mathbf{U}_i = \mathbf{B}_{tot}/|\mathbf{B}_{tot}| = (u_{x_i}, u_{y_i}, u_{z_i})$ around which the spin is precessing and is given for a single trajectory by [12]

$$R_i = \begin{pmatrix} \cos(\frac{\alpha_i}{2}) - iu_{z_i}\sin(\frac{\alpha_i}{2}) & (-iu_{x_i} - u_{y_i})\sin(\frac{\alpha_i}{2}) \\ (-iu_{x_i} + u_{y_i})\sin(\frac{\alpha_i}{2}) & \cos(\frac{\alpha_i}{2}) + iu_{z_i}\sin(\frac{\alpha_i}{2}) \end{pmatrix}. \tag{5.5}$$

After each scattering event the electron will precess around a new effective magnetic field, and we follow the quantum mechanical spin evolution in the total effective magnetic field during each ballistic trajectory. The rotation operator along the entire trajectory can be represented as the product of the individual operators along the n straight sections of the trajectory

$$R = R_n \cdots R_2 R_1. \tag{5.6}$$

We thus find the spin state of each electron as a function of time.

The spin evolution is calculated for an ensemble of (at least) 10^3 electrons. This mimics the averaging over many electrons in an electron transport experiment, since large quantum dots behave in practice as a chaotic ballistic cavity [13]. In our model the magnitude of the average spin orientation for the ensemble decays to zero because each electron has its own scattering trajectory, such that the relative difference between the precessional dynamics of individual electrons increases in time. We will always refer to this as spin relaxation for the ensemble (with decay time T_1), rather than dephasing, because we concentrate on the loss of average spin orientation in the direction of the external magnetic field that we apply. Note however, that in our description each individual electron always keeps precessing coherently in its particular spin-orbit field. Consequently, the underlying mechanism is equivalent to that of spin dephasing for an ensemble,

and in particular for our simulations with $B_{ext} = 0$ T one could argue that the loss of spin orientation should be named dephasing.

The average spin orientation is calculated for the whole ensemble as a function of time, independent of the position of the individual electrons. In this study we concentrate on the average spin polarization $\langle S_x \rangle$ in the $\hat{\mathbf{x}}$-direction. We find in all cases that we consider here that the decay time for $\langle S_x \rangle$ equals that of $\langle S \rangle$, where $\langle S \rangle = \sqrt{\langle S_x \rangle^2 + \langle S_y \rangle^2 + \langle S_z \rangle^2}$, because no significant polarization develops in the $\hat{\mathbf{y}}$ or $\hat{\mathbf{z}}$-direction. The relaxation time T_1 is then defined as the time when $\langle S_x \rangle$ is reduced to $1/e$ of its initial value at $t = 0$. We used electron density $1.0 \cdot 10^{15}$ m^{-2} and mobility 100 m^2/Vs, unless stated otherwise. We neglect inelastic scattering mechanisms and electron-electron interactions.

The momentum direction for an electron changes after specular scattering on the boundary of the system. This process we will refer to as edge scattering and the typical length scale involved here is L, where the area of the quantum dot system is $A = L^2$. A second effect causing a change in momentum direction is scattering on static fluctuations in the potential due to impurities. Here, a scatter event changes the momentum into a random direction. We incorporate this into our modeling as follows. When an electron is moving ballistically through the system, the probability that it did *not* scatter due to impurities decreases as e^{-t/τ_s} (where τ_s is the average impurity scatter time) and this probability is reset to 1 after each impurity scatter event. We thus define the mean free path $L_{mfp} = |v_F|\tau_s$ as the length in between scatter events when only considering impurity scattering.

Another important length scale in our system is the so-called precession length $\langle L_{pr} \rangle$. This is defined as the length of the trajectory where a spin has precessed over an angle π. In our system this length scale is k-vector dependent due to the anisotropy of SO fields. Therefore, we define $\langle L_{pr} \rangle$ as the length of the trajectory for precession over an angle π around the average total effective magnetic field $\langle |\mathbf{B}_{tot}| \rangle$, where we average over all k-directions to account for the anisotropy for the SO contribution to the total field.

Evaluating the relative size of these three length scales, L, L_{mfp}, and $\langle L_{pr} \rangle$, for a specific system helps to understand many properties of the relaxation time. Before discussing results for quantum dots, it is instructive to discuss two regimes that occur for a free 2DEG (L very large). For such systems, Fig. 5.3 presents traces with T_1 as a function of L_{mfp}. We first focus on the case with $B_{ext} = 0$ T, for which $\langle L_{pr} \rangle = 8$ μm. If $L_{mfp} \ll \langle L_{pr} \rangle$, the precession angle in between scatter events is small. Consequently, the spin state only slowly diffuses away from

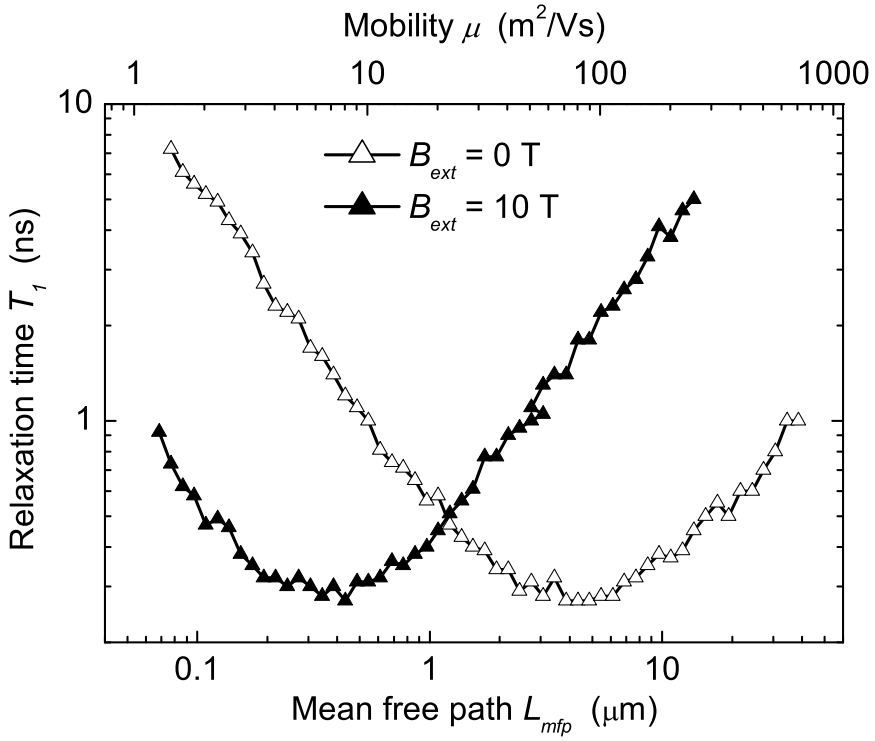

Figure 5.3: Relaxation time T_1 as a function of the mean free path L_{mfp} for a free 2DEG. The top axis shows the corresponding value for mobility μ. Calculations for zero external field and $B_{ext} = 10$ T.

its initial direction in a random walk-like process. Here scattering suppresses relaxation. This regime is known as the motional narrowing regime [22], and the relaxation time is inversely proportional to the scatter time, $T_1 \propto \tau_s^{-1}$. When $L_{mfp} \gg \langle L_{pr} \rangle$, the spins will coherently precess over at least one full rotation between scatter events. Without momentum scattering, the ensemble shows spin relaxation since each electrons precesses in a different field, but each electron will maintain its component in the direction of its precession axis. Only when a scatter event occurs this coherent precession is disturbed, such that further relaxation for the ensemble can occur. In this regime $T_1 \propto \tau_s$. The crossover between these two regimes (where T_1 shows a minimum) occurs for $L_{mfp} \approx \langle L_{pr} \rangle$. Switching on an external magnetic field of 10 T for this system, reduces the length scale $\langle L_{pr} \rangle$ to 1.1 μm. For T_1 as a function of L_{mfp}, this only results in a shift of the entire curve, with the minimum now occurring at the new value where $L_{mfp} \approx \langle L_{pr} \rangle$. We conclude here that our calculations for Fig. 5.3 reproduce the conventional result [2].

5.4 Results

We now turn to discussing results for quantum dots, for which L can be smaller than $\langle L_{pr} \rangle$ and L_{mfp}. Figure 5.1a shows simulations of the relaxation time as a function of dot size L. We first discuss the result for zero external magnetic field (which gives $\langle L_{pr} \rangle = 8$ μm) and mobility $\mu = 100$ m^2/Vs (corresponding to $L_{mfp} = 5$ μm). For this system, a decrease of L in the regime with $L < \langle L_{pr} \rangle$ results in higher T_1 values. We will refer to this regime as the quasi-0D regime. Here frequent scattering suppresses precession, as for motional narrowing in the 2D regime. Here, we observe that $T_1 \propto L^{-2}$, a dependence on L that was also found for studies on the suppressed relaxation in long quasi-1D channels of width L [8, 23]. For $L > \langle L_{pr} \rangle$ we do not observe any change in T_1. This will be denoted as the 2D regime, for which $L \gg \langle L_{pr} \rangle, L_{mfp}$.

For $B_{ext} = 10$ T (and again $\mu = 100$ m^2/Vs) the behavior is dramatically different (also shown in Fig. 5.1a). When coming from the 2D regime, there is no longer simply an increase in T_1 when lowering L towards the regime where $L \ll \langle L_{pr} \rangle, L_{mfp}$. Instead, there is a regime, here for 0.6 μm $< L <$ 10 μm, where T_1 is strongly suppressed. Moreover, the decrease in T_1 when lowering L from 10 μm to 1 μm shows a structured pattern. For this value of the external magnetic field the precession length is reduced to $\langle L_{pr} \rangle = 1.1$ μm. The mean free path is still $L_{mfp} = 5$ μm, such that switching on a strong field opens up a regime with $\langle L_{pr} \rangle \lessapprox L < L_{mfp}$ in between the 2D and the quasi-0D regimes. Notably, switching on a strong magnetic field for a system in the 2D regime increases T_1 by about one order of magnitude. However, switching on a field for a system in the same material with $L \approx 1$ μm causes T_1 to go down more than 2 orders of magnitude. Now confinement enhances relaxation.

For $B_{ext} = 0$ T and $\mu = 100$ m^2/Vs we do not see a dependence of T_1 on L in the regime where $L > \langle L_{pr} \rangle$, because for that system $L_{mfp} \approx \langle L_{pr} \rangle$. However, also in zero external magnetic field we can open up a regime where $\langle L_{pr} \rangle \lessapprox L < L_{mfp}$ by choosing a higher value for mobility. This is demonstrated for $\mu = 1000$ m^2/Vs (which gives $L_{mfp} = 50$ μm) in Fig. 5.1a. Now for 7 μm $< L <$ 100 μm the relaxation time decreases when decreasing L, and again T_1 shows a structured pattern (*i.e.* the structure on this trace here is not noise from averaging over a finite ensemble).

The reduction in T_1 due to stronger confinement is thus a general effect and appears whenever $\langle L_{pr} \rangle \lessapprox L < L_{mfp}$. These are typical conditions for micronscale quantum dots when large external magnetic fields are applied. Notably, the values

that we obtain here for T_1 are very close to the values that we recently observed in spin accumulation experiments in micronscale quantum dots [13]. We found $T_1 \approx 300$ ps for a quantum dot with $L \approx 1.1$ μm and $B_{ext} = 8.5$ T. This indicates that our simulations generate realistic numbers.

We will now analyze the relaxation mechanism for this confinement-enhanced relaxation. To study why there is strong dip and structure in the dependence of T_1 on L, we choose a simplified model system where we only consider the Rashba SOI and an external magnetic field $B_{ext} = 10$ T. Both Dresselhaus SOI contributions have been set to zero. Using only Rashba has the advantage that the magnitude for the SO fields is identical for all k-vectors. The structure in T_1 appears more regular here (see Fig. 5.1b). This proves that the effects that we present here do not only occur for very particular SO parameters.

We have repeated this calculation where we programmed non-specular reflections on the walls of the quantum dot, such that after hitting a side of the quantum dot the electron is reflected with random angle back into the quantum dot (open symbols in Fig. 5.1b). The structure on T_1 still appears, which confirms that self-repeating patterns are not the origin of this effect. We observe, however, that the amplitude of the structure on T_1 is reduced for this setting. This is caused by an increased variation in the length of trajectories in between scatter events for non-specular reflections. We checked this by making histograms of the trajectory lengths for specular and non-specular reflections (not shown).

For both traces in Fig. 5.1b, we find that the minimums in T_1 appear at odd multiples of the average precession length $\langle L_{pr} \rangle$, and local maximums occur at even multiples of $\langle L_{pr} \rangle$. This means that for systems with a size equal to an odd multiple of $\langle L_{pr} \rangle$ the electrons scatter (on average) after precessing (again, on average) over an angle of exactly π (mod 2π) between scatter events, furthest away from their original state. This causes fast relaxation. For systems with a size equal to an even multiple of $\langle L_{pr} \rangle$, the electrons scatter on average after precessing 2π (mod 2π), so when they are back in their original state. Then relaxation is slower as compared to the local minimums. However, note that for these local maximums there is overall still a reduction of T_1 due to confinement as compared to free 2DEG: in this regime, more frequent scattering on the edge of the system always enhances relaxation. The character of the relaxation mechanism itself is thus similar to the regime with $\langle L_{pr} \rangle \ll L_{mfp}$ for 2D systems, where $T_1 \propto \tau_s$. The additional feature here is the structure on T_1 as a function of L, which signals that the overall relaxation mechanism is either somewhat resonantly enhanced or suppressed when the time-of-flight across the dot matches even or odd multiples

of the spin precession time for an angle π. Notably, the results for free 2DEG in the regime with $T_1 \propto \tau_s$ (Fig. 5.3) do not show structure on T_1 because there is a larger spread in the scatter times τ_s. We checked that when we program that impurity scattering in a random direction always occurs after a fixed time τ_s (no spread), we also observe structure on T_1 as a function of L_{mfp} for a free 2DEG (not shown).

The most extreme suppression of T_1 due to confinement is in ballistic quantum dots ($L \ll L_{mfp}$) when the size of the system $L = \langle L_{pr} \rangle$. Figure 5.2c indicates that this is a counter-intuitive result when this condition is met in strong external fields. The various precession axes get more and more aligned when the external field is increased to 10 T in $\hat{\mathbf{x}}$-direction, while the spins are prepared in this direction. Nevertheless, the lowest T_1 value that occurs for the various traces in Fig. 5.1a is for a quantum dot system of $L = 1.1$ μm in a field of $B_{ext} = 10$ T. Due to the initial spin state in the $\hat{\mathbf{x}}$-direction, spins are initially precessing with relatively small cone angles around these effective magnetic fields, and all electrons will maintain a large component in the $\hat{\mathbf{x}}$-direction. This results only in a small reduction of $\langle S_x \rangle$. Further relaxation for the ensemble only progresses when spins hop onto wider precession cone angles, which only occurs at a scatter event. Thus, more scattering leads to more rapid relaxation, in particular when L is an odd multiple of $\langle L_{pr} \rangle$, and most rapidly when $L = \langle L_{pr} \rangle$. The reason that this results in a very fast relaxation mechanism for small systems in strong magnetic fields is that the precession and scatter times that underlie this mechanism are then very short.

5.5 Conclusions

In conclusion, we have shown that the relaxation time T_1 for a spin population in a certain 2DEG material can be strongly decreased when bringing the size of the system from free 2DEG down to micronscale quantum dots. The strongest suppression is found for ballistic systems of a size L that equals the precession length $\langle L_{pr} \rangle$. Here, frequent scattering on the edge of the dot rapidly drives precession onto wider and wider cone angles, and this effect is resonantly enhanced in all systems where L equals an odd multiple of $\langle L_{pr} \rangle$. We believe our results are very useful for comparison to experimental results on this type of systems, since we can use realistic device and SO parameters. Furthermore, the T_1 values that we calculate match very well with our recent experimental results on micronscale quantum dots as presented in Chapter 4 of this thesis [13].

We thank M. J. van Veenhuizen, A. I. Lerescu, J. Liu and T. Last for useful discussions. This work was supported by the Dutch Foundation for Fundamental Research on Matter (FOM) and the Netherlands Organization for Scientific Research (NWO). During the preparation of this manuscript we became aware of similar work underway by S. Lüscher *et al.* [24].

References

[1] For a recent review see R. H. Silsbee, J. Phys.: Cond. Mat. **16**, R179 (2004).

[2] For a recent review see J. Fabian, A. Matos-Abiague, C. Ertler, P. Stano, I. Zutic, Acta Physica Slovaca **57**, 565 (2007); arXiv:0711.1461 (2007).

[3] S. Datta and B. Das, Appl. Phys. Lett **56**, 665 (1990).

[4] I. Ẑutić, J. Fabian, and S. Das Sarma, Rev. Mod. Phys. **76**, 323 (2004).

[5] D. D. Awschalom and M. E. Flatté, Nature Phys. **3**, 153 (2007).

[6] M. I. D'yakonov and V. I. Perel', Sov. Phys. JETP **33**, 1053 (1971); Sov. Phys. Solid State **13**, 3023 (1972).

[7] M. I. D'yakonov and V. Y. Kachorovskii, Sov. Phys. Semicond **20**, 110 (1986).

[8] A. A. Kiselev and K. W. Kim, Phys. Rev. B **61**, 13115 (2000).

[9] R. Hanson *et al.*, Rev. Mod. Phys. **79**, 1217 (2007).

[10] A. V. Khaetskii and Y. V. Nazarov, Phys. Rev. B **61**, 12639 (2000).

[11] A. V. Khaetskii and Y. V. Nazarov, Phys. Rev. B **64**, 125316 (2001).

[12] C. Cohen-Tannoudji, B. Diu, and F. Laloë, *Quantum Mechanics* (John Wiley and Sons, New York, 1977), p. 698.

[13] E. J. Koop *et al.*, arXiv:0801.2699 (2008).

[14] S. M. Frolov *et al.*, arXiv:0801.4021 (2008).

[15] J. B. Miller *et al.*, Phys. Rev. Lett. **90**, 076807 (2003).

[16] R. M. Potok *et al.*, Phys. Rev. Lett. **89**, 266602 (2002).

[17] J. A. Folk *et al.*, Phys. Rev. Lett. **86**, 2102 (2001).

[18] B. I. Halperin *et al.*, Phys. Rev. Lett. **86**, 2106 (2001).

[19] Cheng-Hung Chang, A. G. Mal'schukov, and K. A. Chao, Phys. Rev. B **70**, 245309 (2004).

[20] Y. A. Bychkov and E. I. Rashba, Sov. Phys. JETP, **39**, 78 (1984).

[21] G. Dresselhaus, Phys. Rev. **100**, 580 (1955).

[22] C. P. Slichter, *Principles of Magnetic Resonance*, Springer series in Solid-State Sciences Vol. 1, 3rd ed. (Springer-Verlag, Berlin, 1989), p. 213.

[23] A. G. Mal'shukov and K. A. Chao, Phys Rev. B **61**, R2413 (2000).

[24] S. Lüscher, S. M. Frolov, and J. A. Folk (unpublished).